DALTON
FULL PAPER

Ionic structure in caustic aluminate solutions and the precipitation of gibbsite

Helen R. Watling,[a] Sean D. Fleming,[b] Wilhelm van Bronswijk[b] and Andrew L. Rohl[b]

[a] *A. J. Parker Cooperative Research Centre for Hydrometallurgy, CSIRO Division of Minerals, PO Box 90, Bentley, Western Australia 6982*
[b] *A. J. Parker Cooperative Research Centre for Hydrometallurgy, School of Applied Chemistry, Curtin University of Technology, PO Box U 1987, Perth, Western Australia 6845*

Received 23rd September 1998, Accepted 9th October 1998

The structure of caustic aluminate solutions in relation to the precipitation of gibbsite was investigated using vibrational spectroscopy and molecular dynamics simulations. Results from the molecular dynamics simulations indicate that aluminate ions form clusters as a function of time and that these clusters are stabilised by sodium ions. While the method used has the limitation that bond formation is forbidden, the predicted clustering would certainly facilitate polyaluminate anion formation. It is proposed that observed additional bands in vibrational spectra of concentrated aluminate solutions, as compared with those of dilute solutions, result from vibrations of these clusters (and any polyaluminate ions which arise from them). The absence of spectral features characteristic of a distinct interfacial aluminate layer at the growing crystal surface is explained by clustering throughout the bulk solution, and the participation of such clusters (and polyanions) in the growth process.

Historically, comparisons have been made between vibrational spectra of solutions and those of aluminate compounds as a means of describing aluminate ion structures. Most authors concur with the interpretation of Moolenaar *et al.*[1] that monomeric $Al(OH)_4^-$ ions exist in equilibrium with $[(OH)_3AlOAl(OH)_3]^{2-}$, the dimeric hydroxo ion.[2–4] This conclusion is consistent with ^{27}Al-solution NMR results which show that most of the aluminium in caustic aluminate solution has four-fold coordination.[5,6] However, to limit the aluminate species distribution to the above two anions may be too narrow a view. Gibbsite, which is known to precipitate spontaneously from pure, homogeneous caustic solutions supersaturated with aluminium,[7] has a complex structure in which aluminium atoms have six-fold coordination and are linked to one another by double hydroxo bridges in a hexagonal layered structure.[8] Clearly the spontaneous precipitation of gibbsite from solution must involve further changes in anionic structure (four-fold to six-fold aluminium coordination and oxo to hydroxo bridging) together with the formation of oligomeric intermediate species.

There is little doubt that geometries calculated *via* quantum mechanics, with the subsequent prediction of vibrational frequencies, has been useful in describing the S_4 symmetry of the $Al(OH)_4^-$ monomeric ion.[9,10] However, attempts to model other aluminate ions in solution are less convincing, perhaps because *ab initio* calculations for gas phase molecules are not entirely suitable for the assignment and interpretation of spectra of related solution species, or because researchers are predisposed towards Moolenaar's[1] "dimer" hypothesis. For example, quantum chemical calculations[11,12] have been used to explain the ultraviolet spectra of sodium aluminate solutions (or *vice versa*) in terms of three anions, $Al(OH)_4^-$, $Al_2O(OH)_6^{2-}$ and $Al(OH)_6^{3-}$; however, the UV spectrum of an aluminate solution arises from the soluble impurities rather than the aluminate ions in solution,[13] which casts doubt on the authors' interpretation.

The simulation of liquids, one of the earliest applications of computer chemistry,[14] has been developed to the point where it is now possible to simulate complex behaviour in complex solutions by using periodic cells containing of the order of several hundred atoms.[15] Many recent studies on the nature of aqueous solutions have been accomplished using molecular dynamics. For example, Levitt *et al.*[16] attempted to construct a model (mainly suitable for use with macromolecules) which would reproduce selected physical properties of water. Laaksonen *et al.*,[17] who investigated the methane–water system, demonstrated the use of molecular dynamics to generated spatial distribution functions which describe the local solution structure. Mancera *et al.*[18] focused on the effect of temperature on the aggregation of methane in aqueous solution. For ionic systems, ion selectivity was examined by plotting the free energy profile of cations to a crown ether in water,[19] while the hybrid QM/MM technique was used to show that a solely classical approach was inadequate to describe the solvation of calcium ions in water.[20]

In this study, vibrational spectroscopy is combined with molecular dynamics simulations to investigate possible ion associations in aluminate solutions (synthetic Bayer liquors), at concentrations of industrial relevance. [The Bayer process is the most widely used method for the production of gibbsite, $Al(OH)_3$, which is then calcined to alumina and electrolytically reduced to aluminium.] The results are discussed in relation to the mechanism of gibbsite crystal growth.

Experimental

Spectroscopy

Caustic solutions were prepared using analytical grade sodium, potassium and caesium hydroxides. Aluminate solutions were prepared by dissolving aluminium wire (BDH product 10006) in the hot caustic solutions; the resulting liquors were filtered through 0.45 μm pore size membranes and diluted to volume with hot distilled water. Final solution concentrations were determined using inflection point titrimetry.[21]

Infrared spectra were collected at 4 cm^{-1} resolution using a Bruker IFS-66 spectrometer, with DTGS detector, equipped with an Axiom Dipper-210 ATR probe with zinc selenide element. The useful working range was estimated to be 4000–600 cm^{-1}. Raman spectra of crystallizing solutions were collected at 4 cm^{-1} resolution using a Bruker Near-Infrared RFS100 FT spectrometer, with NdYAG-1064 nm laser excitation (900 mW) and Ge-diode detector.

Raman polarisation measurements were made on an ISA Labram 1B dispersive spectrometer using HeNe excitation (14 mW) and a 600 lines mm^{-1}, giving a resolution of ≈2.7 cm^{-1}. Bands due to solvent and caustic solution were removed from aluminate solution spectra by subtracting the spectra of equivalent caustic solutions. Subtraction was deemed satisfactory when a straight baseline was obtained in the region of interest (450–800 cm^{-1}). Both subtracted and unsubtracted spectra were used to calculate polarisation ratios, and gave similar results.

Molecular modeling

The molecular dynamics simulations reported in this paper were conducted on Silicon Graphics workstations, using the Discover package from Molecular Simulations Incorporated, San Diego. The ESFF potential set[22] was chosen to represent all force field interactions, since the system contains two metallic atom types in addition to oxygen and hydrogen. The Verlet velocity method was employed to integrate the equations of motion. All simulations were conducted with the use of periodic boundary conditions, with the Ewald technique[23] employed to evaluate the van der Waals, and the coulomb interactions.

Three systems were constructed, each possessing a composition similar to that of a synthetic Bayer liquor (7 $[Al(OH)_4]^-$, 5 OH^-, 12 Na^+ and 192 H_2O molecules). For each simulation, the molecules of the system were placed in a cubic lattice, the dimensions of which were selected to avoid overlap. A randomising algorithm was used to choose the location and orientation of each component whilst preserving the overall required ratio of species. Several hundred 1 fs steps at high pressure in an NPT ensemble (with velocity scaling temperature control) were then undertaken to obtain simulated liquors with the expected density. This gave cubic simulation boxes of approximately equal dimensions ($L \approx 18.5$ Å), corresponding to a solution with $[Al(OH)_3] \approx 1.8$ M, $[NaOH] \approx 3.2$ M and a density of approximately 1.2 g cm^{-3}. These concentrations are similar to that of a synthetic Bayer liquor at 80 °C.[24]

The final configurations of these simulations were then used as the starting point for a further 500,000 cycles (step size 1 fs) in an NVT ensemble. The first 200 ps were taken as an equilibration period, with data collection in the final 300 ps. The more robust Andersen temperature control method[15] was used for the equilibration while the more realistic Berendsen method[14] was used for the data collection.

Results

Spectroscopy of aluminate solutions

Raman spectra were obtained for caustic and aluminate solutions (Na, K, Cs) with a range of compositions (Fig. 1, Table 1). These exhibit the expected one- or three-band spectra for aluminate ion Al–O vibrations in the low-frequency region.

A feature of the Raman spectra collected during an initial study[25] was the increased asymmetry and width of the side-bands (≈695 and ≈535 cm^{-1}) which flank the most intense aluminate band attributed to $Al(OH)_4^-$ (≈620 cm^{-1}).[1] This, together with the observed shifts in band frequency at maximum intensity with changed solution composition, tended to support the hypothesis that each side band resulted from two or more vibrations of similar frequency.

In the present study, further evidence for this is obtained from spectra of solutions containing one molar aluminium and very high sodium hydroxide concentrations (Fig. 1, g and h). At low caustic concentrations (4 molar) and one molar aluminium, only one aluminate band is observed (≈620 cm^{-1}), as expected; at this aluminium concentration the side bands are not apparent. However, a low intensity band centred at 555 cm^{-1} becomes apparent in solution spectra as the caustic concentration is increased to 19 molar. This is not the same band as that which appears in spectra of concentrated aluminate solutions (≈535 cm^{-1}), and which exhibits a significant shift to lower frequencies as the aluminium concentration is increased (at constant caustic concentration) (Fig. 1f). The appearance of the low intensity 555 cm^{-1} band is consistent with the formation of small concentrations of $Al(OH)_6^{3-}$ in these extremely caustic solutions, but such a hypothesis needs to be confirmed by independent methods.

In an attempt to resolve the side bands (≈695 and ≈535 cm^{-1}) into their components, depolarization ratios for each of them were determined, the rationale being that not all component vibrations need have the same degree of symmetry (Table 1).

Table 1 Calculated depolarisation ratios, ρ, for aluminate ion vibrational bands

Aluminate solution	ρ ≈695 cm^{-1}	ρ ≈620 cm^{-1}	ρ ≈535 cm^{-1}
5M $NaAl(OH)_4$ 3M NaOH excess	≈0.25	0.02	0.02
4M $NaAl(OH)_4$ 6M NaOH excess	≈0.20	0.025	0.025
4M $KAl(OH)_4$ 6M KOH excess	≈0.15	0.02	0.02
3M $NaAl(OH)_4$ 2M NaOH excess	≈0.20	<0.01	<0.01
3M $KAl(OH)_4$ 2M KOH excess	≈0.3	<0.01	<0.1
3M $CsAl(OH)_4$ 2M CsOH excess	≈0.3	<0.01	<0.1
1M $NaAl(OH)_4$ 4M NaOH excess	—	<0.01	—
1M $NaAl(OH)_4$ 18M NaOH excess	—	0.03	<0.1[a]

[a] 555 cm^{-1} band.

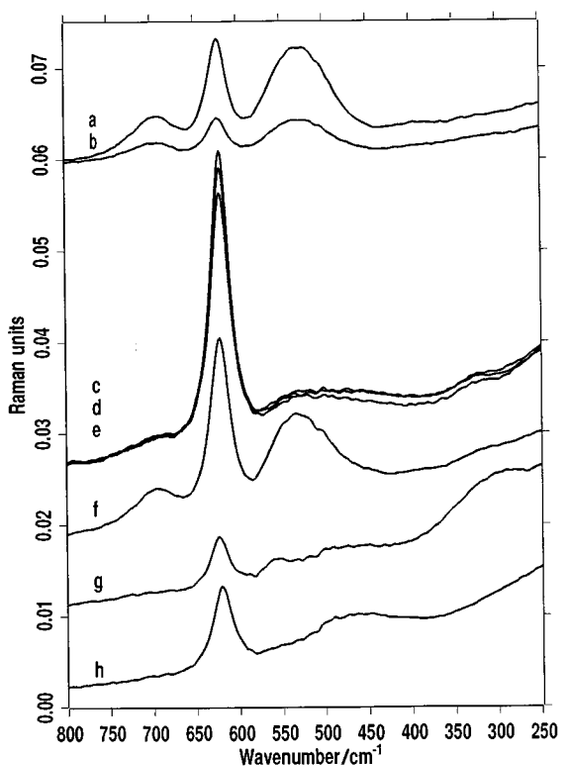

Fig. 1 Raman spectra of aluminate solutions as recorded. a,b) Polarised and depolarised spectra, 5M sodium aluminate with 3M excess NaOH; c,d,e) Cs, K and Na aluminate solutions all 3M in aluminate with 2M excess caustic; f) 5M sodium aluminate with 3M excess NaOH; g) 1M sodium aluminate with 18M excess NaOH; h) 1M sodium aluminate with 4M excess NaOH.

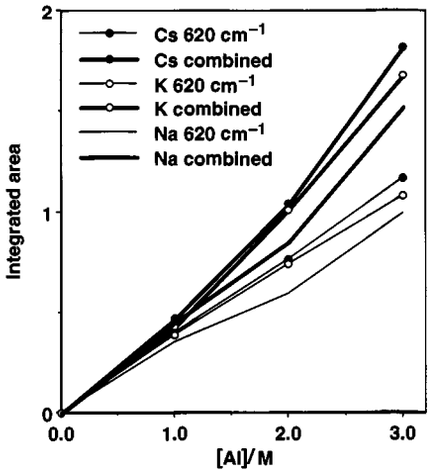

Fig. 2 Integrated areas of aluminate Raman-active vibrational bands (combined 535, 620 and 695 cm^{-1} and 620 cm^{-1}) for sodium, potassium and caesium aluminate solutions with total cation concentration 5M.

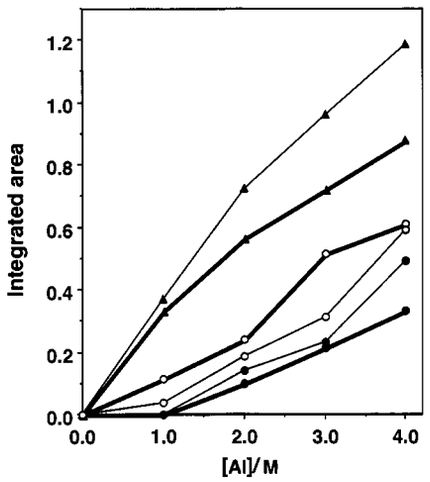

Fig. 3 Integrated areas of aluminate Raman-active vibrational bands in spectra of concentrated solutions (total cation concentration 10M). Cations ▮ = Na and | = K; frequencies ▲ = 620 cm^{-1}, ● = 695 cm^{-1} and ○ = 535 cm^{-1}.

At the same time the effects of possible cation–aluminate ion pairing on spectra were investigated using a series of aluminate solutions prepared with sodium, potassium or caesium hydroxides.

In respect of depolarization ratios, illustrated for a sodium aluminate solution (Fig. 1, a and b), it is significant that all three bands in the Raman spectrum of an aluminate solution are the result of symmetrical bond vibrations, irrespective of solution concentration or cation. Only one of them, the 620 cm^{-1} band, can be attributed to the aluminate monomer $Al(OH)_4^-$ which has S_4 symmetry.[10] The other bands must arise from one or more additional aluminate species (*new species*) in equilibrium with the monomer in concentrated aluminate solutions. Unfortunately, although the degree of fit obtained by modeling of the spectra is such as to suggest that each of the side bands has more than one component, all components were shown to have a strong degree of symmetry and differences in polarised spectra did not enable the deconvolution of the bands.

Raman spectra of alkali metal hydroxides also exhibit a very broad low-intensity, low-frequency band at ≈300 cm^{-1} which has been attributed to $MOH{\cdot}H_2O$, in which an almost symmetric O–M–O linkage exists.[26] The intensity of this band is reduced when aluminium is introduced into solution, a feature which has been interpreted as indicating that cation affinity is greater for the aluminate ion than for the hydroxide ion.[27] Aluminate and hydroxide solution spectra collected in the present study confirm the above observations and are consistent with the interpretation (Fig. 1, g and f).

The effects of the different cations on aluminate vibrational bands are small (Fig. 1, c, d and e). Apart from a systematic decrease in the 620 cm^{-1} band intensity accompanied by a small increase in width at half height in the order Na > K > Cs (Fig. 2), spectra are remarkably similar across the full frequency range. This relationship is reflected in the combined area under the curve (three bands) for these spectra. Comparisons between spectra of sodium, potassium and caesium aluminate solutions indicate that, if these spectral differences are due to cation–aluminate ion pairing, then pairing is strongest in the sodium system.

Bands associated with aluminate ion vibrations were modeled and integrated areas for the three bands were determined for concentrated solutions of sodium and potassium aluminates (Fig. 3). Consistency is achieved in that, across the aluminium concentration range investigated, the observed decrease in the 620 cm^{-1} band area for sodium relative to potassium (at equal aluminium concentration) can be correlated with an increased area in the 535 cm^{-1} band. Thus it appears that one or more *new species* are promoted at the expense of the aluminate ion in sodium solutions compared with potassium solutions.

Results from the previous study[25] had led to the belief that both the 535 and 695 cm^{-1} bands arose from vibrations of the same *new species*, so that changes in the 695 cm^{-1} band area should correlate with those of the 535 cm^{-1} band. This does not seem to be the case, but the analysis should be interpreted with caution because this is the least well defined of the three bands under investigation, which introduces a significant error into the model.

The gibbsite–aluminate interface

Concentrated alkaline aluminate solutions supersaturated with aluminium are inherently unstable. From the time of preparation changes take place in these solutions which will result in the precipitation of bayerite (a gibbsite polymorph formed at ambient temperature) or gibbsite (>60 °C). In an attempt to monitor these changes, Raman spectra of a freshly prepared, filtered solution were collected as a function of time until precipitation occurred (Fig. 4, a and b). Only bands attributable to the aluminate solution or to bayerite were observed when precipitation occurred and no changes in solution spectra were observed up to that point.

However, in the same time frame, the intensity of the Rayleigh line increased significantly (Fig. 5). Indeed, this was the only evidence of any changes taking place in the solution and is attributed to increased Rayleigh scattering by small particles which are being formed. As Rayleigh scatter is proportional to a particle's polarisability it increases as a function of the square of the volume, *i.e.* the sixth power of its diameter.[28] However, as the number of particles decreases, with the formation of fewer, larger aggregates, the intensity is expected to increase as a function of the square of the diameter of the particle for simple aggregation (*i.e.* monomer, dimer, tetramer, *etc.*). Rayleigh scatter is the major scattering mechanism when the particle diameter (D) is less than approximately one twentieth of the wavelength (λ) being scattered. As the diameter of the particles increases the Rayleigh–Gans region, $0.1 < D/\lambda < 1$, is reached and the 180° back scatter intensity reduces relative to the forward scatter, until at $D \cong \lambda$ the back scatter intensity is typically less than one tenth of the forward scatter.[28] The observed initial rapid increase in Rayleigh scatter (Fig. 5) is thus as expected for particle growth and the subsequent decrease in rate indicates that the Rayleigh–Gans region has been reached, or that the rate of particle growth has slowed.

Attenuated total reflectance (ATR) infrared spectroscopy

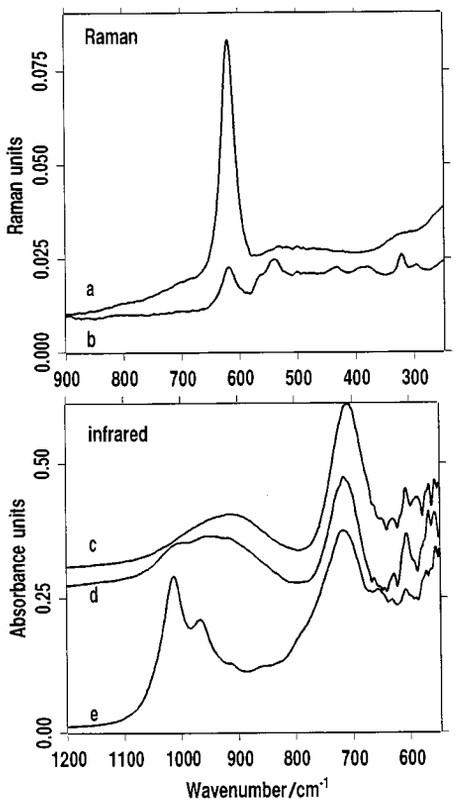

Fig. 4 Raman and infrared spectra obtained from interface studies. a,b) Initial Raman spectrum of a supersaturated sodium aluminate solution and that obtained as precipitation commenced; c) infrared spectrum of freshly prepared sodium aluminate solution; d,e) spectra collected of a gibbsite slurry and of the solution through a layer of gibbsite scale.

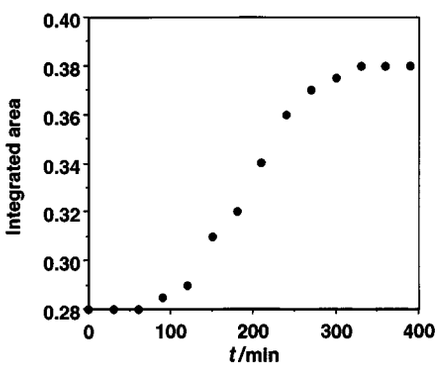

Fig. 5 Rayleigh scattering as a function of time (state of aggregation).

was used to study the gibbsite aluminate solution interface in aqueous solution. Spectra were obtained of supersaturated aluminate solutions (60 °C) using one of two configurations (Fig. 6). In the first, the ATR element was immersed in a slurry of gibbsite particles under conditions known to promote gibbsite crystal growth; in this way the interface was sampled through the solution at the particle surface (Fig. 6a). In the second, a layer of gibbsite scale was deposited on the ATR element, which was then immersed in a solution, again under conditions which would promote further gibbsite deposition onto the scale layer (Fig. 6b). Here, the interface was sampled through the gibbsite scale. With either configuration, the spectrum collected is representative of solution and gibbsite 1–2 μm from the ATR element and must include both the interfacial layer at the growing crystal surface and bulk solution.

Spectra collected from both experiments (Fig. 4, c, d and e) are interesting in that they exhibit only those bands associated with aluminate solutions and those associated with gibbsite. In addition, solution infrared spectra collected using a trans-

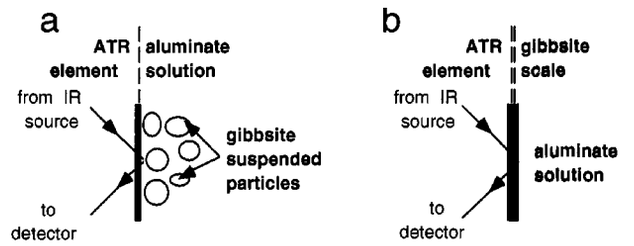

Fig. 6 ATR-FTIR study of the gibbsite–aluminate ion interface. a) Sampling the gibbsite surface through the aluminate solution; b) sampling the aluminate solution through a gibbsite scale layer.

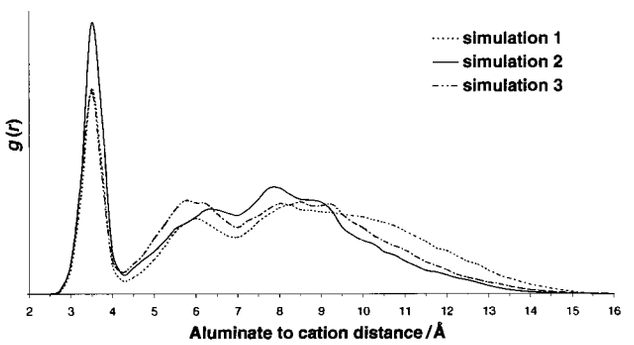

Fig. 7 Aluminate to sodium radial distribution functions for the data collection period.

mission cell are identical with those collected using the ATR probe. No spectral features have been identified that can be attributed to an interfacial aluminate layer which is distinguishable from the bulk solution.

Molecular dynamics simulations

During the 300 ps data collection period, the coordinates of all atoms in the simulation cells were stored at intervals of 100 fs. Thus, each simulation yielded 3000 cell snapshots, or frames, which were analysed for sodium and aluminate structuring.

The first measurements made were the distances from the centre of each aluminate ion to all the sodium cations. Analysis of this data yielded the sodium aluminate radial distribution function (RDF) shown in Fig. 7. In order to attach some significance to the result, the RDFs for the first few hundred steps of the equilibration period were constructed for each simulation; these plots contained no significant peaks. Hence the peaks in Fig. 7, which occur at an aluminate to cation separation of around 3.5 Å, are the result of ion pairing.

While the RDFs for simulation 1 and simulation 3 exhibit very similar behaviour, the second simulation experiences a greater degree of ion pairing. In addition, past the first large peak in the RDFs, the rest of the distributions appear to possess additional smaller peaks. While these are not as distinct, the deviation from a smooth curve suggests that some longer range solution structuring is also occurring.

Further investigation was facilitated by the construction of radial distribution functions for aluminate Al–Al separations (Fig. 8). As in the case of the previous plot, the initial RDF for the equilibration period of each simulation exhibited no prior structuring. In Fig. 8, all three distributions possess a peak at around 5 Å, although it is evident that simulation 2 experiences the greatest degree of aluminate 'clustering'. It is these clustered aluminates, each with their own shell of paired cations, that are responsible for the smaller peaks in Fig. 7.

In Fig. 9, we have constructed a graph of the number of cations paired with each aluminate, *versus* the proportion of occurrence. This data was obtained by recording the number of cations paired to each aluminate, and summing over every frame in the data collection period. Thus, we normalise the

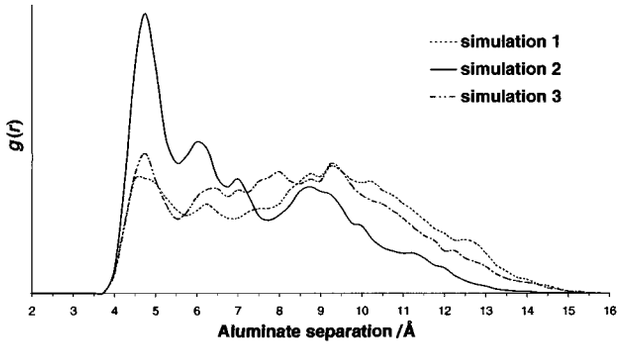

Fig. 8 Aluminate separation radial distribution functions for the data collection period.

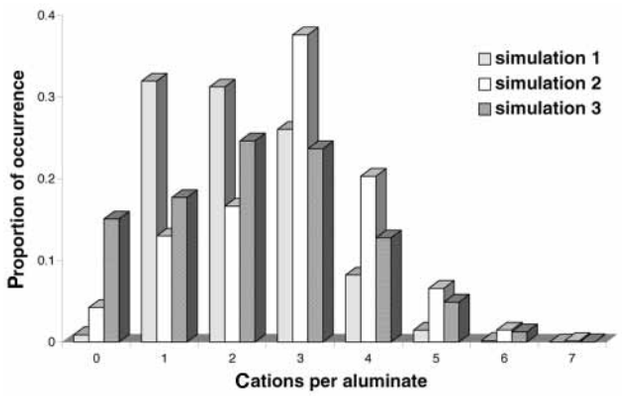

Fig. 9 The extent of simulation time (data collection period) for which the aluminates experience different numbers of paired cations. An ion pair is judged as having a separation of no greater than 4.1 Å.

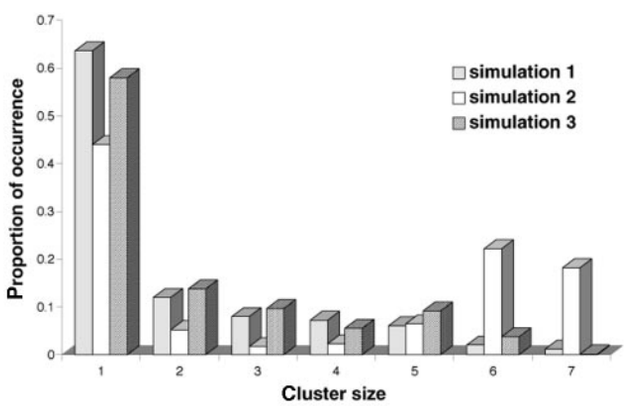

Fig. 10 The extent of simulation time (data collection period) which each aluminate spends in different sized clusters. A cluster is a group of linked aluminate ions, with a separation less than 5.5 Å.

graph with the product of the number of aluminate ions (7) and the number of frames (3000). In addition, with the use of Fig. 7, we have defined a paired cation as being closer than 4.1 Å to the Al atom of an aluminate ion.

The data in Fig. 9 indicate that the aluminate ions in simulations 1 and 3 are paired to an average of between two and three cations. For simulation 2, there is a large proportion of aluminates with three or more associated cations. As each cell has a composition of 7 aluminates and 12 sodiums, the cations are clearly being shared by multiple aluminate ions which have come into proximity. This is particularly evident in simulation 2.

Further information emerges from the aluminate cluster size distribution shown in Fig. 10. A cluster is defined as a group of linked aluminate monomers with Al–Al separations of not more than 5.5 Å. The data was collected by cumulatively recording the size of the cluster each aluminate belongs to in each simulation frame. Thus, the distribution was normalised with the same value employed to normalise the data in Fig. 9.

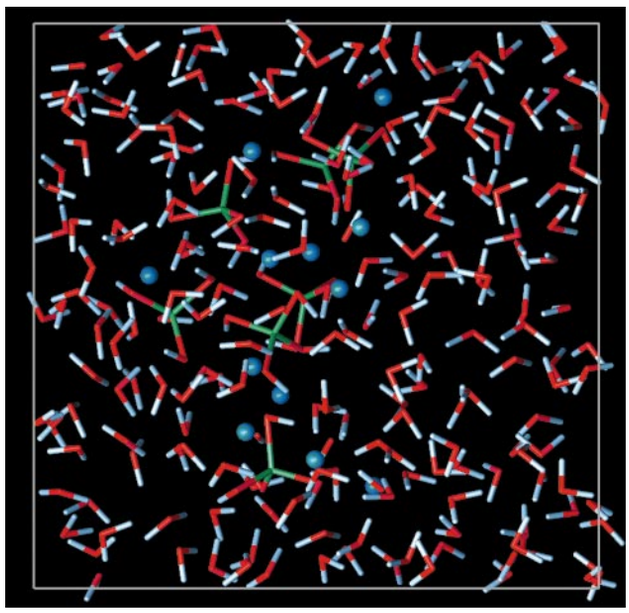

Fig. 11 A snapshot of simulation 2 at 200 ps through the data collection period. This illustrates the maximal clustering of all seven aluminates.

This figure suggests that simulations 1 and 3 experience relatively small amounts of aluminate clustering, with a large fraction of aluminates remaining 'isolated' during the simulation. However, the second simulation has formed very large clusters that are stable enough to account for almost half of the simulation time. As the second simulation also possesses the highest number of shared cations, it is clear that these sodium–-aluminate bridges are playing an important role in the formation of clusters.

The data used to generate Fig. 9 was examined in order to establish how the number of paired cations changes as a function of time. This analysis indicated that, in general, the cations associated with an aluminate are not rigidly bound. Thus, throughout the entire simulation, there is a random fluctuation in the number of cations paired with a particular aluminate. The mean value of these oscillations in associated cations was reported earlier as being between two and three. This mobility of the bridging cations is an important feature, and may have implications in the formation of polyaluminate species.

Collectively, the data in Fig. 7 to 10 may be thought to indicate that the sodium and aluminate ions evolve, from initial isolation, into subsequently larger and larger groups. These groups being characterised by the ion pairing and clustering discussed previously. This implies that, if given sufficient time, the simulations would exhibit the form seen in Fig. 11, where all aluminates are bound into a 'super' cluster. However, this is not the case.

An examination of the changes in cluster sizes during the data collection period, has indicated that simulations 1 and 3 experience varying oscillations in both the sizes and proportions of all clusters. This is also evident in the proportions of isolated aluminates, which fluctuates from between 40% to 80% for each frame, and only overall yielding an average of around 60% (*cf*. Fig. 10). Thus, at some simulation point, the numbers and sizes of all clusters present are randomly distributed, and not proportional to the age of the simulation.

An analysis of the individual motions of cations for each simulation was conducted. This revealed that, in simulation 2, a stable cluster of size 7 was formed from a size 6 cluster at approximately two thirds the way through the data collection period. Whilst the formation of the larger cluster was preceded by an intake of cations, the cluster subsequently underwent a

period of stabilisation, coinciding with a steady increase in the number of free cations in solution.

This size 7 cluster in simulation 2 dominated the cell for around 80 ps. However, by the end of the data collection period it had broken up into smaller units. This confirmed the earlier observation that there is no correlation between the age of the simulation and the cluster size distribution. In addition, as cluster destruction and new groupings of monomers occur continuously throughout the simulation, the aluminate–aluminate binding energy must be less than the thermal energy.

Discussion

The reaction for the dissolution of bauxite or the precipitation of gibbsite from hot alkaline aluminate solutions in the Bayer Process is often represented as

$$Al(OH)_4^- \overset{NaOH}{\rightleftharpoons} Al(OH)_3 + OH^-$$

but this equation fails to indicate the complexity of even the simplest case where gibbsite nuclei $(Al(OH)_3)_n$ form spontaneously in a supersaturated aluminate solution. Homogeneous gibbsite nucleation must involve processes such as (i) ordering of aluminate ions in solution, (ii) formation of hydroxo-bridges between Al atoms, (iii) a change from four- to six-fold Al coordination geometry, (iv) release of sodium and hydroxyl ions from the nucleating crystal to the bulk solution, a consequence of which is (v) the separation of solid phase from solution (dehydration).

Even in the Bayer process, where solutions are seeded and growth consists mainly of the incremental addition of gibbsite to seed crystal surfaces (during agglomeration, growth and secondary nucleation), aluminate ions must undergo similar changes with the consequent release of hydroxyl and sodium ions to solution. Thus, any mechanism that is proposed for the precipitation of gibbsite must account for these processes, while being consistent with experimental observations.

The data collected in the present study contribute mainly to an understanding of solution ordering.

Observed changes in spectra with increasing concentration, such as frequency shifts at maximum intensity and loss of proportionality with band intensities,[25] and the appearance of new vibrational bands or the increased asymmetry in the shape of existing ones (all of which are shown to be symmetric vibrations), cannot be explained on the basis of the monomer or its sodium ion pair. Thus it is concluded that, while the monomeric $Al(OH)_4^-$ ion or its sodium ion pair predominates in dilute aluminate solutions, at least one new species, presumably a polyaluminate, forms in concentrated solutions.

While the structures of such polyaluminate species cannot be described solely on the basis of the spectroscopic data, it is expected that the aluminium coordination in them remains four-fold and aluminium atoms are linked by oxo-bridges. The maximum concentration of $Al(OH)_4^-$ is estimated to occur at ≈4–5 molar aluminium in solution, above which concentration the new species become relatively more abundant at the expense of the monomer.[25]

Results obtained from the molecular dynamics simulation tend to support the spectroscopic evidence. Whereas it has been assumed that monomeric $Al(OH)_4^-$ ions would be distributed randomly (homogeneously) in solution, the simulations predict that they aggregate into clusters which are stabilised by sodium ions. Analysis has also indicated that the sodium ions are quite mobile with excess cations being ejected from the cluster as it stabilises.

The main limitation of the simulation method used is that bonds cannot be formed or broken. So that, although aluminate monomers are predicted to form clusters, facilitating the formation of polyaluminate species, no information about either the bonding between aluminate ions or the aluminium geometry is obtained. However, as noted above, one of the intermediate steps in gibbsite precipitation involves the release of sodium ions to the bulk solution. This may already be partly accomplished through the predicted clustering mechanism.

The interfacial layer at the surface of a seed crystal is indistinguishable, spectroscopically, in structure from that of the bulk solution. There are no significant changes in vibrational spectra of aluminate solutions, in the Al–O band frequency region, during the induction period leading to the spontaneous precipitation of gibbsite. An underlying assumption concerning the interface experiments was that such a layer with a "different" structure should exist, and thus the inability to detect it was due to the insensitivity of the spectroscopic technique. However, if aluminate clusters are formed in the bulk solution as predicted, and if these participate in the growth of gibbsite on seed crystal surfaces, the absence of characteristic changes in spectra of the interfacial layer are explained. The additional sidebands in spectra of concentrated aluminate solutions are representative of both polyaluminate clusters in solution and at the gibbsite–solution interface where they participate in the growth process.

The one significant change in spectra collected during the induction period up to the point where particles were visible as a faint suspension was the increased intensity of Rayleigh scattering. Recent additional data from multiangle laser light scattering (MALLS)[29] also showed a progressive increase in light scattering prior to the appearance of suspended particles, consistent with a nucleation mechanism. In that case, particles were estimated to be ≈180 nm diameter, but according to Rossiter *et al.*[7] this might be an overestimation. The estimated diameter is approximately one sixth of the wavelength of the laser used (1064 nm) and confirms that the increased scattering reported in Fig. 5 is due to the Rayleigh and Rayleigh–Gans phenomena and that the Tyndall scattering region ($D > \lambda$) has not been reached. The important point is that such particles could not form if the aluminate ion clustering, as predicted by the simulation, did not take place.

Conclusion

The data obtained from a spectroscopic study of caustic aluminate solutions supersaturated with aluminium during the period leading up to the spontaneous nucleation of gibbsite in them, and of the gibbsite–solution interface in seeded aluminate solutions, have been interpreted with the aid of molecular dynamics simulations of a solution of equivalent composition.

Predictions from the molecular dynamics simulations include the clustering of aluminate ions in solution, and the stabilisation of these clusters by sodium ions. A limitation of the method is that bond formation is not permitted, but the predicted clustering would certainly facilitate polyaluminate anion formation.

It is thought that the additional spectral bands observed in Raman and infrared spectra of concentrated aluminate solutions are due to vibrations of these clusters (and any polyaluminate anions which form from them). The absence of spectral features characteristic of a distinct interfacial aluminate layer at the growing crystal surface is explained by clustering throughout the bulk solution, and the participation of such clusters (and polyanions) in the growth process.

Acknowledgements

We would like to thank Professor C. R. A. Catlow for invaluable discussions on the modelling techniques used in this work. The financial support of the Australian Government through its Cooperative Research Centres Program is also gratefully acknowledged.

References

1 R. J. Moolenaar, J. C. Evans and L. D. McKeever, *J. Phys. Chem.*, 1970, **74**, 3629.
2 N.-Y. Chen, M.-X. Liu, Y.-L. Cao, B. Tang and M. Hong, *Sci. in China*, *Ser. B*, 1993, **36**, 32.
3 L. A. Myund, V. M. Sizyakov, M. K. Khripun and A. A. Makarov, *Russian J. Gen. Chem.*, 1995, **65**, 826; *Zh. Obshch. Khim.*, 1995, **65**, 911.
4 L. A. Myund, V. M. Sizyakov, K. A. Burkov, V. O. Zakharzhevskaya and O. A. Borzenko, *Russian J. Gen. Chem.*, 1995, **68**, 1721; *Zh. Obshch. Khim.*, 1995, **68**, 1964.
5 J. W. Akitt and W. Gessner, *J. Chem. Soc.*, *Dalton Trans.*, 1984, 147.
6 J. W. Akitt, W. Gessner and M. Weinberger, *Magn. Reson. Chem.*, 1988, **26**, 1047.
7 D. S. Rossiter, P. D. Fawell, D. Ilievski and G. M. Parkinson, *J. Cryst. Growth*, 1998, **191**, 521.
8 H. Saalfeld and M. Wedde, *Z. Kristallogr.*, 1974, **139**, 129.
9 E. R. Lippincott, J. A. Psellos and M. C. Tobin, *J. Chem. Phys.*, 1952, **20**, 536.
10 A. C. Hess, P. F. McMillan and M. O'Keefe, *J. Phys. Chem.*, 1988, **92**, 1785.
11 H. Liu, S. Huang and N. Chen, *Trans. Nonferrous. Met. Soc. China*, 1992, **2**(3), 43.
12 N. Chen and H. Liu, *J. Mol. Struct.* (*THEOCHEM.*), 1994, **305**, 283.
13 P. Sipos, P. M. May, G. T. Hefter and I. Kron, *J. Chem. Soc.*, *Chem. Commun.*, 1993, 2355.
14 D. Frenkel and B. Smit, *Understanding Molecular Simulation*, Academic Press, San Diego, CA, 1996.
15 M. P. Allen and T. D. Tildesley, *Computer Simulation of Liquids*, Oxford University Press, Oxford, 1997.
16 M. Levitt, M. Hirshberg, R. Sharon, K. E. Laidig and V. Daggett, *J. Phys. Chem. B*, 1997, **101**, 5051.
17 A. Laaksonen, P. G. Kusalik and I. M. Svishchev, *J. Phys. Chem. A*, 1997, **101**, 5910.
18 R. L. Mancera, A. D. Buckingham and N. T. Skipper, *J. Chem. Soc.*, *Faraday Trans.*, 1997, **93**, 2263.
19 L. X. Dang, *J. Am. Chem. Soc.*, 1995, **117**, 6954.
20 A. Tongraar, K. R. Liedl and B. M. Rode, *J. Phys. Chem. A*, 1997, **101**, 6299.
21 G. Woods, H. Watling and P. Smith, *Analysis of Bayer type liquors by inflection point titrations*, CSIRO Division of Mineral Products Confidential Report No IR/P-001, 1994.
22 S. Barlow, A. L. Rohl, S. G. Shi, C. M. Freeman and D. O'Hare, *J. Am. Chem. Soc.*, 1996, **118**, 75.
23 D. M. Heyes, *J. Chem. Phys.*, 1981, **74**, 1924.
24 A. S. Russell, J. D. Edwards and C. S. Taylor, *J. Met.*, 1955, **7**, 1123.
25 H. Watling, *Appl. Spectrosc.*, 1998, **52**, 250.
26 M. Moskovits and K. H. Michaelian, *J. Am. Chem. Soc.*, 1980, **102**, 2209.
27 S. K. Sharma and S. C. Kashyap, *J. Inorg. Nucl. Chem.*, 1972, **34**, 3623.
28 T. Allen, *Particle size measurement*, Chapman and Hall, London, 4th edn., 1990, p. 487.
29 P. D. Fawell and H. R. Watling, *Appl. Spectrosc.*, 1998, **52**, 1115.

Paper 8/07420H